Mass balance of the Sør Rondane glacial system, East Antarctica

Denis CALLENS,[1] Nicolas THONNARD,[1] Jan T.M. LENAERTS,[2] Jan M. VAN WESSEM,[2] Willem Jan VAN DE BERG,[2] Kenichi MATSUOKA,[3] Frank PATTYN[1]

[1]*Laboratoire de Glaciologie, Université Libre de Bruxelles, Brussels, Belgium*
[2]*Institute for Marine and Atmospheric Research Utrecht, Utrecht University, Utrecht, The Netherlands*
[3]*Norwegian Polar Institute, Tromsø, Norway*
Correspondence: Denis Callens <dcallens@ulb.ac.be>

ABSTRACT. Mass changes of polar ice sheets have an important societal impact, because they affect global sea level. Estimating the current mass budget of ice sheets is equivalent to determining the balance between surface mass gain through precipitation and outflow across the grounding line. For the Antarctic ice sheet, grounding line outflow is governed by oceanic processes and outlet glacier dynamics. In this study, we compute the mass budget of major outlet glaciers in the eastern Dronning Maud Land sector of the Antarctic ice sheet using the input/output method. Input is given by recent surface accumulation estimates (SMB) of the whole drainage basin. The outflow at the grounding line is determined from the radar data of a recent airborne survey and satellite-based velocities using a flow model of combined plug flow and simple shear. This approach is an improvement on previous studies, as the ice thickness is measured, rather than being estimated from hydrostatic equilibrium. In line with the general thickening of the ice sheet over this sector, we estimate the regional mass balance in this area at $3.15 \pm 8.23\,\mathrm{Gt\,a^{-1}}$ according to the most recent SMB model results.

KEYWORDS: accumulation, atmosphere/ice/ocean interactions, ice-sheet mass balance, radar-echo sounding

INTRODUCTION

Precise knowledge of the mass balance of ice sheets is essential for estimating their contribution to current and future sea-level rise. The numerous assumptions necessary to assess the global mass balance of Antarctica lead to significant discrepancies between the estimates (Rignot and others, 2011a; Zwally and Giovinetto, 2011). The Ice Mass Blance Inter-comparison Exercise (IMBIE) consortium (Shepherd and others, 2012) reconciled results from a range of different methods (input/output method (IOM), satellite altimetry and gravimetry) to determine that the average mass loss of the entire Antarctic ice sheet over the period 1992–2010 was $71 \pm 53\,\mathrm{Gt\,a^{-1}}$. During this period, the East Antarctic ice sheet (EAIS) mass change may be positive ($+14 \pm 43\,\mathrm{Gt\,a^{-1}}$), while the West Antarctic ice sheet (WAIS) and Antarctic Peninsula ice sheet (APIS) lost mass (-65 ± 26 and $-20 \pm 14\,\mathrm{Gt\,a^{-1}}$, respectively). While the magnitude of change of the WAIS and APIS are therefore relatively well constrained, even the sign of the sea-level rise contribution from the EAIS remains uncertain.

A significant issue of mass change estimation is that none of the methods presently used are free from significant errors, and all rely on either models or approximations (Shepherd and others, 2012). The IOM calculates the balance between the total surface mass balance (SMB) that feeds a given drain-age basin and the loss of ice through ice discharge at the basin outlet (e.g. Rignot and others, 2008). Satellite gravimetry and altimetry (e.g. Gunter and others, 2009) measure the absolute mass change but rely on a glacial isostatic adjustment (GIA) model, while altimetry also suffers uncertainty due to the densification process. As most of the drainage basins in the EAIS are close to equilibrium (Shepherd and others, 2012), these methods

struggle to provide good estimates, because a small error in the GIA model will introduce large relative errors in the results (Hanna and others, 2013).

Nevertheless, a recent IOM study (Zwally and Giovinetto, 2011) emphasizes that the IOM is equally prone to a large uncertainty. Indeed, the method is highly sensitive to the choice of the SMB as an input parameter. At present, several SMB datasets are available, either based on regional atmospheric modelling (Van de Berg and others, 2006; Van Wessem and others, 2014) or on data assimilation methods (Arthern and others, 2006). Lenaerts and others (2012) compare several datasets and identify a discrepancy up to 15%, which is $>300\,\mathrm{Gt\,a^{-1}}$ for the whole Antarctic ice sheet.

The IOM has another pitfall. When no thickness data are available, the flux gate is set seaward of the grounding line, with the ice thickness then derived from the ice surface elevation. This method assumes that the glacier reaches hydrostatic equilibrium a few kilometres beyond the grounding line and that ice thickness does not change significantly between the grounding line and the point where the ice shelf actually freely floats. However, these can be separated by several kilometres, so this assumption may not be correct. For instance, along the Princess Ragnhild Coast, East Antarctica, the grounding line and hydrostatic line are $\sim 2\,\mathrm{km}$ apart (Bindschadler and others, 2011). Within this interval, under the Pine Island Ice Shelf, intense subglacial melting of up to several tens of metres per year can occur at the seaward side of the grounding line (Payne and others, 2007; Dutrieux and others, 2013) and may represent an important sink of mass which will affect the mass-balance estimation. This is one order of magnitude higher than the local SMB and will introduce a significant error into the mass-balance calculations. Moreover, any
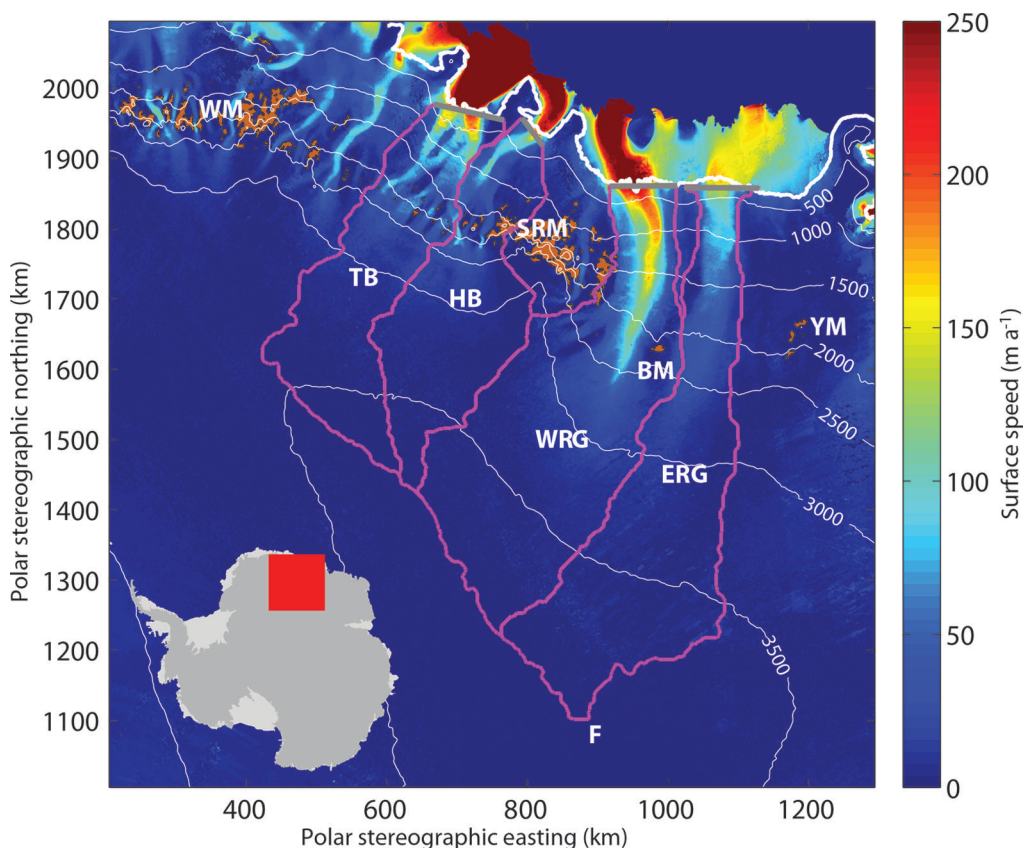
Fig. 1. Map of the Sør Rondane Mountains glacial system, Antarctica. Background colour shows the surface flow speed (Rignot and others, 2011a). Contours show surface elevations (Bamber and others, 2009). The four drainage basins are in purple. Their downstream section (grey curve) is the output gate used to determine the basin extension and the outflux. These are the gates surveyed by the radar and presented in Figure 2. Rock outcrops are shown in brown (SCAR, 2012). White curve is the grounding line (Bindschadler and others, 2011). SRM: Sør Rondane Mountains; WM: Wohlthat Massif; BM: Belgica Mountains; YM: Yamato Mountains; F: Dome Fuji. The glacier acronyms are TB: Tussebreen; HB: HE Hansenbreen; WRG: West Ragnhild Glacier; ERG: East Ragnhild Glacier. With exception of HE Hansenbreen, none of these glacier names are official, but a number of them have been frequently used in the literature (e.g. Pattyn and others, 2005).

error in ice-shelf surface elevation is multiplied by a factor of ten when translated into ice thickness. An alternative to this approach is to calculate the outflow slightly upstream of the grounding line. Unfortunately, this can lead to two potential problems: (1) if radar measurements are not available, there is no remote-sensing method to estimate the thickness of the grounded ice and (2) ice dynamics must now be considered, since the independence of flow speed with depth (plug flow) is no longer valid.

Within the eastern Dronning Maud Land (DML) sector of the EAIS, only a limited number of glaciological studies have been carried out. Van Autenboer and Decleir (1978) estimated the mass balance of the glaciers in the Sør Rondane Mountains (SRM), but their study was limited to the smaller glaciers within the mountain range, and does not include the primary ice flow outlets that flow through and are diverted around the major coastal mountain systems. On a continental scale, a number of studies have established the mass balance of DML drainage basins. The most recent such studies are those of Rignot and others (2008) and Shepherd and others (2012). Along the Princess Ragnhild Coast, Rignot and others (2008) base their analysis on the flux through the ice shelf, where ice thickness is determined from hydrostatic equilibrium. Shepherd and others (2012) assume the ice sheet in this area to be in equilibrium, since thickness data at the grounding line are lacking. In the meantime, GRACE

(Gravity Recovery and Climate Experiment; gravimetry) and ICESat (Ice, Cloud and land Elevation Satellite; altimetry) reconstruction of the mass budget do not agree in eastern DML (Gunter and others, 2009).

In this paper, we present the first estimate of the mass balance of the entire SRM glacial system using IOM. To avoid bias associated with the assumption of hydrostatic equilibrium, we base our calculations on data from an airborne radar survey which determined the ice thickness of the outlet gates slightly upstream of the grounding line. We then compare different datasets of SMB to investigate the impact of SMB uncertainties on the overall result.

GEOGRAPHICAL SETTING

The SRM glacial system consists of four large outlet glaciers which flow from the Dome Fuji ice divide toward the Princess Ragnhild Coast, DML (Fig. 1). West of the SRM are Tussebreen (TB) and HE Hansenbreen (HB; both between the Wohlthat Massif and the SRM). To the east, there are West Ragnhild Glacier (WRG; Pattyn and others, 2005; Callens and others, 2014) between SRM and the Belgica Mountains, and East Ragnhild Glacier (ERG) between the Belgica and Yamato Mountains. The position of these glaciers, and the surface flow speed (Rignot and others, 2011b) are shown in Figure 1.
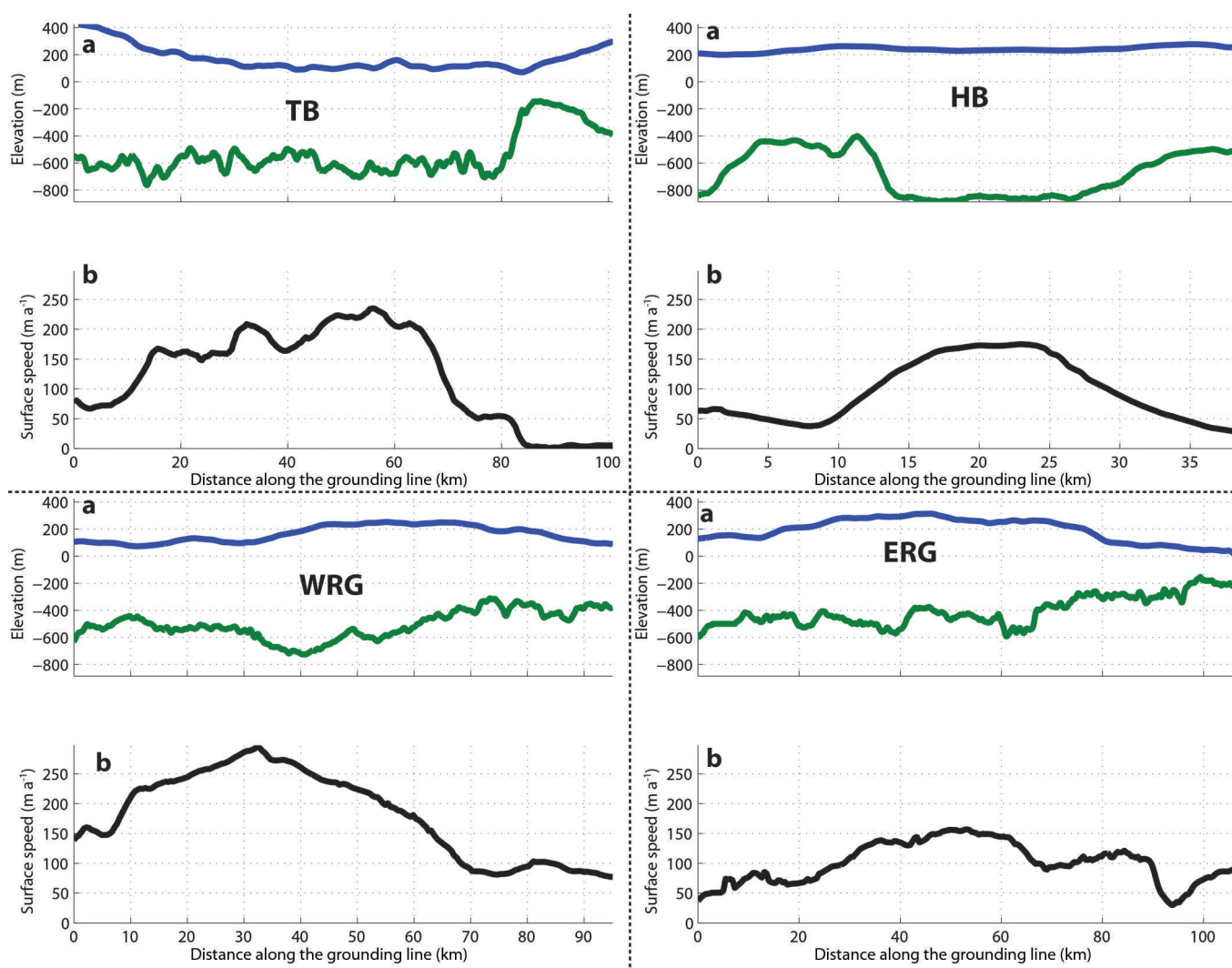
Fig. 2. (a) Geometry and (b) velocity profiles along the flux gate of each glacier, oriented west to east. The flux gates are chosen along the closest flight track to the grounding line. In (a) the blue curve is the surface elevation and the green curve is the bed elevation. In (b) the black curve is the surface speed (Rignot and others, 2011a). TB: Tussebreen; HB: HE Hansenbreen; WRG: West Ragnhild Glacier; ERG: East Ragnhild Glacier.

METHODS

Ice thickness measurements

To map the ice thickness at the grounding line, an airborne radio-echo sounding survey was carried out in the area during the 2010/11 austral summer (Callens and others, 2014). The survey consisted of a series of cross-flow profiles, of which one was taken close to the grounding line of each of the glaciers (Fig. 1), as well as a longitudinal profile along the flowline. The radar system employed a 150 MHz centre frequency (Nixdorf and others, 1999; Steinhage and others, 2001). The system recorded at a rate of 20 Hz. For further signal-to-noise improvement, the data were stacked tenfold, resulting in a horizontal resolution of 80 ± 20 m.

Ice thickness was derived using a constant radio-wave propagation speed of 168 m μs^{-1}. The uncertainty in the thickness estimation is approximately ± 30 m (Steinhage and others, 1999). Surface elevation was obtained by laser altimetry from the aircraft, and bed elevation was subsequently derived by subtracting the ice thickness from the surface elevation. We applied the geoid height of 20 m above the EGM96 ellipsoid (Rapp, 1997) to derive the

surface and bed elevations relative to sea level (these data are available on Pangaea, doi: 10/1594/PANGAEA.836299).

The cross-profile geometry and the ice flow speeds are displayed in Figure 2.

Surface mass balance

We determine the outlines of each drainage basin by back-tracking flowlines from the outflux gate boundaries near the grounding line in the upstream direction. (The determination of the flux gates is given in the next subsection.) Starting from the grounding line, we trace flowlines on a surface digital elevation model (Bamber and others, 2009), until their convergence at the ice divide. We assumed that ice follows the steepest surface slope. A second step consists of integrating the SMB over each of the drainage basins. The SMB datasets used are those of Van de Berg and others (2006), Arthern and others (2006) and Van Wessem and others (2014); they are hereafter referred to as B06, A06 and W14 respectively. A06 is a dataset based on interpolation of ground-based observations (spanning 1950–2000), with a satellite-derived distribution. B06 is derived from the Regional Atmospheric Climate Model version 2 (RACMO2) at ~55 km spatial resolution, driven by the European Centre for Medium-Range

Weather Forecasts' ERA-40 reanalysis (1980–2004), and calibrated using ground-based measurements. W14 is also derived from RACMO2, on ~27 km spatial resolution, driven by ERA-Interim reanalysis (1979–2013), without any a posteriori output calibration. We assume that the mean SMB values over these periods represent these SMB models, and use them for the IOM calculations.

Outflow

The flux gates are defined along flight tracks of the airborne radar survey. The aim is to cover a maximum of the flux within the limitations of the radar survey (Fig. 2). However, as long as the basin is determined by the flux gate, all the ice flowing through the flux gate is supposed to have accumulated in the associated basin. Since we prescribe the gate width, no errors are associated with this quantity.

To estimate ice flux, we use the surface velocities of Rignot and others (2011b), taken upstream of the grounding line and coinciding with the airborne radar profiles. The velocities are projected perpendicular to these flight lines, to account for the fact that the flowline is not exactly perpendicular to them: the norm of the velocity vector is multiplied by the cosine of the angle between the normal of the gate and the velocity vector.

When the flux gate is set seaward of the grounding line, it is common to assume that ice flow speed is independent of depth (plug flow) (Rignot and others, 2008):

$$\Phi = \int_w^e U_{\perp s}(y) H(y)\, \mathrm{d}y, \tag{1}$$

where Φ is the ice flux, $U_{\perp s}(y)$ denotes the surface speed perpendicular to the flux gate (Rignot and others, 2011b), H is the thickness, y the cross-flow direction and w and e denote the western and eastern boundaries of the gate. However, in this study, we set the flux gate on the grounded ice, where the ice flow speed can vary with depth, depending on the deformational characteristics. To assess mass-balance uncertainty associated with the flow regime, we consider different possible types of flow. First, we assume a plug-flow regime, Eqn (1), where the mean ice flow speed equals the surface flow speed. Second, we introduce a combined plug/simple-shear flow regime, in which the ice flow speed depends both on internal deformation and basal motion. For this purpose, we use the simplest way to describe ice flow according to simple shear, i.e. based on the shallow-ice approximation:

$$\overline{U}_{\perp d}(y) = \frac{2\varepsilon\overline{A}}{n+2} H(y)\tau_d^n(y), \tag{2}$$

where $\overline{U}_{\perp d}$ is the depth-averaged deformational speed and $\tau_d(y) = -\rho g H(y)|\nabla z_s|$ is the driving stress. Other parameters in Eqn (2) are $\overline{A}$ and n, the depth-integrated temperature-dependent flow parameter and the exponent in Glen's flow law, respectively. ε is the enhancement factor, ρ is the ice density, g is the gravitational acceleration and z_s is the surface elevation. Following Cuffey and Paterson (2010), $\varepsilon = 3$, $n = 3$ and $\overline{A} = 3.5 \times 10^{-25}$ Pa^{-3} s^{-1}, so that $\overline{A}$ corresponds to a mean englacial temperature of −10°C. Finally, the surface gradient, ∇z_s, is derived from laser altimetry at the flowline, and we assume that it is constant along the grounding line cross section, so that ice thickness, H, is the only spatially varying parameter in Eqn (2). In order to reduce flow-coupling effects on short spatial scales, the surface

gradients are calculated over approximately ten times the ice thickness (Kamb and Echelmeyer, 1986).

Once $\overline{U}_{\perp d}$ is determined, basal sliding, $U_{\perp b}$, is taken as the difference between it and the observed surface velocity. For the shallow-ice approximation, this becomes (Cuffey and Paterson, 2010)

$$U_{\perp b}(y) = U_{\perp s}(y) - \frac{n+2}{n+1}\overline{U}_{\perp d}(y). \tag{3}$$

The total mass outflux at the grounding line is thus a combination of the flux driven by basal motion and the flux driven by internal deformation. This type of flow is hereafter called hybrid flow:

$$\Phi = \int_w^e \left[U_{\perp b}(y) H(y) + \overline{U}_{\perp d}(y) H(y) \right] \mathrm{d}y. \tag{4}$$

Error calculation

For the SMB datasets W14 and B06, the uncertainty in modelled SMB is derived from a comparison with 153 available SMB observations over the whole of northeastern DML (70–77° S, 0–65° E; Van de Berg and others, 2006). For each of the SMB observations, a comparison with modelled SMB is performed, and the total SMB uncertainty at each location is assumed to be the absolute difference between the two values. This uncertainty can be ascribed to both an uncertainty in observation and in the model. Uncertainties on observed SMB are assumed to be linearly proportional to the SMB itself (e.g. Rignot and others, 2008). The remaining uncertainty, that which is ascribed to the model, is calculated as the square root of the difference between the quadratic total uncertainty and the quadratic observational uncertainty. The resulting 153 model mismatches are then averaged.

Since A06 is based on an interpolation of ground-based SMB measurements, this dataset is not independent of these measurements; in this case, we cannot assume that the A06 error constitutes an independent observational and model error. Therefore we assume a spatially homogeneous error of 10% over the entire basin (Arthern and others, 2006).

In order to calculate error on mass outflux, we only consider the error on the measured quantities: ice thickness, $E_H = \pm 30$ m, and surface flow speed, E_{U_s} (Rignot and others, 2011b). The error on the flux estimation under the assumption of plug flow is given by

$$E_\Phi = \int_w^e \left[E_{U_{\perp s}}(y) H(y) + E_H U_{\perp s}(y) \right] \mathrm{d}y. \tag{5}$$

For hybrid ice flow, error propagation leads to

$$E_\Phi = \sqrt{ \begin{aligned} &\left\{ \int_w^e \left[E_{U_{\perp b}}(y) H(y) + E_H U_{\perp b}(y) \right] \mathrm{d}y \right\}^2 + \\ &\left\{ \int_w^e \left[E_{\overline{U}_{\perp d}}(y) H(y) + E_H \overline{U}_{\perp d}(y) \right] \mathrm{d}y \right\}^2 \end{aligned} }, \tag{6}$$

where

$$E_{U_{\perp b}}(y) = \sqrt{ E_{U_{\perp s}}(y)^2 + E_{\overline{U}_{\perp d}}(y)^2 } \tag{7}$$

and

$$E_{\overline{U}_{\perp d}}(y) = -\frac{2(n+1)\varepsilon\overline{A}}{n+2} [\rho g H(y)|\nabla z_s|]^n H(y)^n E_H. \tag{8}$$

The error on mass balance is the quadratic mean of the error on input and output.

Table 1. Basin extent and flux gate width for the adjacent drainage basins

| Glacier	Area	Gate width
	km^2	km
Tussebreen	64 292	100.8
HE Hansenbreen	61 542	38.3
West Ragnhild Glacier	117 104	95.0
East Ragnhild Glacier	102 125	106.5

RESULTS

Surface mass balance

The backtracking of the flowline produces four large drainage basins, which extend from the grounding lines toward Dome Fuji ice divide (Fig. 1). Table 1 lists the characteristic sizes of each of the drainage basins.

The three mass input estimates are mutually consistent: they are bounded between 30.2 and 32.1 Gt a^{-1}. Their spread is ~6% of the total SMB. Table 2 presents the errors in the estimation. These were calculated following the method described in the previous section and are based on the comparison between results of the model and 153 point measurements in DML. The specific surface mass balance is used in this calculation and is expressed in terms of SMB per area (mm w.e. m^{-2} a^{-1}). For W14, the error in modelled SMB is 19.2 mm w.e. m^{-2} a^{-1}, which corresponds to 26% of the mean of the observations (73.7 mm w.e. m^{-2} a^{-1}). We assigned this relative error to the error on the area-integrated SMB. Therefore, the relative SMB uncertainty is ~26%, which we apply to the entire SRM glacial system and to the individual basins. The agreement of B06 with observations is similar. The error is 21.0 mm w.e. m^{-2} a^{-1}, yielding a relative SMB uncertainty of 28%. Figure 3 shows RACMO2-based SMB datasets (B06 and W14) compared with observations. B06 tends to underestimate SMB at the locations of in situ measurements. The median of the difference between models and observations is −14 mm w.e. m^{-2} a^{-1}, whereas W14 does not mis-estimate, since its median is equal to −2 mm w.e. m^{-2} a^{-1}.

Errors are significantly higher for B06 and W14 than for A06, due to the different methodologies used to calculate the error. For B06 and W14, we compare the model to point measurements and evaluate the discrepancy. The uncertainty on A06 is set to 10%, as stated by Arthern and others
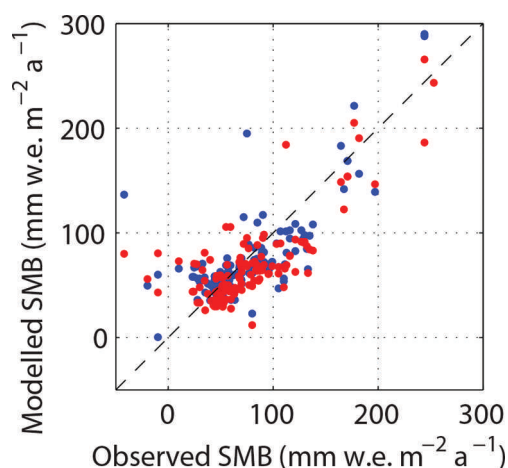
Fig. 3. Comparison of the in situ modelled SMB with observations, with W14 shown in blue and B06 in red. The dashed line is the identity line.

(2006). However, their continent-wide error estimate does not necessarily reflect the local errors.

Outflow

Depending on the assumption made about ice dynamics (plug flow/simple shear), the total outflux varies from 27.55 to 28.32 Gt a^{-1}. The errors were calculated using the method described in Eqns (5–8). They are significantly lower than uncertainties in SMB. At basin level, the mass outflux is a function of the width, the thickness and the flow speed (Eqns (1) and (4)). As revealed by the size of HB, the gate width is a first-order parameter in the calculation of the outflow. However, TB, WRG and ERG have the same width, but the outflow from the latter is 55% of the amount drained by WRG. This large discrepancy is due to the much higher ice flow speed across the grounding line of WRG (and, to a lesser extent, of TB). Ice flow speeds of WRG and TB are up to 298 and 245 m a^{-1}, respectively, while the flow speed of ERG is <152 m a^{-1}.

Concerning the comparison between plug and hybrid flow, the differences remain very small and, in all cases, less than the uncertainties. Therefore, in the mass-balance calculation we will neglect the hybrid flow part and continue by considering only plug flow, because plug flow is the most likely flow type near grounding lines. The low value of ∇z_s (ranging from 11.3×10^{-3} to 18.4×10^{-3}) and the relatively small thicknesses lead to low flux due to

Table 2. Results of the mass budget (Gt a^{-1}) using three different SMBs and two flow regimes. A06, B06 and W14 refer to data of Arthern and others (2006), Van de Berg and others (2006) and Van Wessem and others (2014), respectively

		TB	HB	WRG	ERG	Total
SMB	A06	6.90 ± 0.69	6.50 ± 0.65	10.60 ± 1.06	8.10 ± 0.81	32.10 ± 3.21
	B06	8.20 ± 2.30	4.50 ± 1.26	10.30 ± 2.88	7.20 ± 2.02	30.20 ± 8.46
	W14	8.82 ± 2.29	5.23 ± 1.36	11.03 ± 2.87	6.39 ± 1.66	31.47 ± 8.18
Outflow	Plug flow (PF; Eqn (1))	8.01 ± 0.58	3.31 ± 0.16	10.98 ± 0.50	6.02 ± 0.32	28.32 ± 0.85
	Hybrid flow (Eqn (4))	7.70 ± 0.73	3.22 ± 0.22	10.82 ± 0.61	5.82 ± 0.47	27.55 ± 1.08
Mass budget	A06 − PF	−1.11 ± 0.90	3.19 ± 0.67	−0.38 ± 1.17	2.08 ± 0.87	3.78 ± 3.32
	B06 − PF	0.19 ± 2.37	1.19 ± 1.27	−0.68 ± 2.93	1.18 ± 2.04	1.88 ± 8.50
	W14 − PF	0.81 ± 2.37	1.92 ± 1.37	0.05 ± 2.91	0.37 ± 1.69	3.15 ± 8.23

internal deformation. Indeed, flux due to ice deformation (second term of Eqn (4)) is always one order of magnitude smaller than flux due to basal motion (first term of Eqn (4)). For instance, the former is equal to $0.65\,\mathrm{Gt\,a^{-1}}$ while the latter is $10.17\,\mathrm{Gt\,a^{-1}}$ in the case of WRG.

Mass balance

From the difference between the mass gain through the integrated SMB and the mass loss through the gates, we find that the glacial system is gaining mass slightly, i.e. 1.88–$3.78\,\mathrm{Gt\,a^{-1}}$, depending on the SMB dataset used.

DISCUSSION

The IOM shows consistently large errors for the three SMB datasets used. All datasets give a consistent signal in terms of mass. In general, A06 gives a higher total SMB compared with the datasets based on modelling, but overall results are comparable. B06 and W14 have the same orders of uncertainty, while A06 has a significantly lower error. This is due to the methodology used to ascribe errors to the SMB estimate. We cannot compare A06 with data, since it is an interpolation of them, so we have to rely on the error estimate provided by Arthern and others (2006): maximum 10%. Nevertheless, the errors on SMB represent the majority of the uncertainty for each scenario.

Smallest errors are found on the outflow, as expected: the size of each basin consistently depends on the size of the outflow gate, which has been well defined from the airborne radar data along the grounding line. For the mass outflow, the assumption of plug flow compared with the hybrid approach seems acceptable. The difference between plug flow and hybrid flow is never larger than the calculated uncertainty (Table 2). As shown by Callens and others (2014), ice flow in the downstream section of WRG is primarily governed by basal sliding, so that plug flow is an adequate approximation, which is also true upstream of the grounding line. This statement seems acceptable for the other glaciers, since basal motion dominates the flux. Although the shallow-ice approximation is not intrinsically valid for ice streams, it gives an endmember estimate of how far the results can be from the plug-flow assumption. The comparison supports the use of the assumption. The difference between plug and hybrid flow is never >5%, which is of the order of the magnitude of the error. Indeed, the relatively low surface gradient, ∇z_s, implies a small driving stress, even if the ice is thick, hence it does not influence deformational ice flow. Therefore, the plug-flow assumption can be safely applied here.

Shepherd and others (2012) show that the increasing mass balance observed in this area with GRACE between 2009 and 2011 is driven by a positive accumulation anomaly. However, their study assumed that the basins around SRM are in equilibrium, because of the lack of data to the contrary. Here we estimate mass balance for the mean SMB over the past 34 years (Arthern and others, 2006; Van de Berg and others, 2006; Van Wessem and others, 2014) and outflow based on surface velocities between 2007 and 2009 (Rignot and others, 2011b) and a radar survey made in 2011. Based on these data, the SRM glacial system is slightly gaining mass. Given the mass budget of the EAIS estimated by Shepherd and others (2012) ($+14\,\mathrm{Gt\,a^{-1}}$) and the fact that they assumed equilibrium for the SRM glacial system, our new estimate of its mass budget, ranging from +1.88 to $3.78\,\mathrm{Gt\,a^{-1}}$, increases the continental mass budget by 13–27%, depending on the SMB dataset used. Unfortunately, the large errors due to the SMB uncertainties mean we cannot irrevocably conclude that SRM glacial system mass balance is positive.

CONCLUSIONS

Based on an airborne radar survey along and across the major outlet glaciers of the SRM glacial system, grounding-line ice thickness has been accurately mapped for the major outlet glaciers. We calculated the mass output of the four drainage basins constituted by these glaciers. The outflow was then compared with the mass input from three different SMB datasets, in order to assess their mass balance.

This study gives new insights into the mass balance in DML by contradicting the assumption of equilibrium previously made. According to the latest model and thickness measurements near the grounding line, this part of Antarctica gains $3.15\,\mathrm{Gt\,ice\,a^{-1}}$. However, given the relatively large uncertainties and discrepancies in the SMB, this value needs to be treated with caution.

REFERENCES

Arthern RJ, Winebrenner DP and Vaughan DG (2006) Antarctic snow accumulation mapped using polarization of 4.3 cm wavelength microwave emission. *J. Geophys. Res.*, **111**(D6), D06107 (doi: 10.1029/2004JD005667)

Bamber JL, Gomez-Dans JL and Griggs JA (2009) A new 1 km digital elevation model of the Antarctic derived from combined satellite radar and laser data – Part 1: Data and methods. *Cryosphere*, **3**(1), 101–111 (doi: 10.5194/tc-3-101-2009)

Bindschadler R and 17 others (2011) *High-resolution image-derived grounding and hydrostatic lines for the Antarctic Ice Sheet.* National Snow and Ice Data Center, Boulder, CO. Digital media: http://nsidc.org/data/docs/agdc/nsidc0489_bindschadler

Callens D, Matsuoka K, Steinhage D, Smith B, Witrant E and Pattyn F (2014) Transition of flow regime along a marine-terminating outlet glacier in East Antarctica. *Cryosphere*, **8**(3), 867–875 (doi: 10.5194/tc-8-867-2014)

Cuffey KM and Paterson WSB (2010) *The physics of glaciers*, 4th edn. Butterworth-Heinemann, Oxford

Dutrieux P and 6 others (2013) Pine Island glacier ice shelf melt distributed at kilometre scales. *Cryosphere*, **7**(5), 1543–1555 (doi: 10.5194/tc-7-1543-2013)

Gunter B and 8 others (2009) A comparison of coincident GRACE and ICESat data over Antarctica. *J. Geod.*, **83**(11), 1051–1060 (doi: 10.1007/s00190-009-0323-4)

Hanna E and 11 others (2013) Ice-sheet mass balance and climate change. *Nature*, **498**(7452), 51–59 (doi: 10.1038/nature12238)

Kamb B and Echelmeyer KA (1986) Stress-gradient coupling in glacier flow: I. Longitudinal averaging of the influence of ice thickness and surface slope. *J. Glaciol.*, **32**(111), 267–284

Lenaerts JTM, Van den Broeke MR, Van de Berg WJ, Van Meijgaard E and Kuipers Munneke P (2012) A new, high-resolution surface mass balance map of Antarctica (1979–2010) based on regional atmospheric climate modeling. *Geophys. Res. Lett.*, **39**(4), L04501 (doi: 10.1029/2011GL050713)

Nixdorf U and 6 others (1999) The newly developed airborne radio-echo sounding system of the AWI as a glaciological tool. *Ann. Glaciol.*, **29**, 231–238 (doi: 10.3189/172756499781821346)

Pattyn F, de Brabander S and Huyghe A (2005) Basal and thermal control mechanisms of the Ragnhild glaciers, East Antarctica. *Ann. Glaciol.*, **40**, 225–231 (doi: 10.3189/172756405781813672)

Payne AJ, Holland PR, Shepherd AP, Rutt IC, Jenkins A and Joughin I (2007) Numerical modeling of ocean–ice interactions under Pine Island Bay's ice shelf. *J. Geophys. Res.*, **112**(C10), C10019 (doi: 10.1029/2006JC003733)

Rapp RH (1997) Use of potential coefficient models for geoid undulation determinations using a spherical harmonic representation of the height anomaly/geoid undulation difference. *J. Geod.*, **71**(5), 282–289 (doi: 10.1007/s001900050096)

Rignot E and 6 others (2008) Recent Antarctic ice mass loss from radar interferometry and regional climate modelling. *Nature Geosci.*, **1**(2), 106–110 (doi: 10.1038/ngeo102)

Rignot E, Velicogna I, Van den Broeke MR, Monaghan A and Lenaerts J (2011a) Acceleration of the contribution of the Greenland and Antarctic ice sheets to sea level rise. *Geophys. Res. Lett.*, **38**(5), L05503 (doi: 10.1029/2011GL046583)

Rignot E, Mouginot J and Scheuchl B (2011b) Ice flow of the Antarctic Ice Sheet. *Science*, **333**(6048), 1427–1430 (doi: 10.1126/science.1208336)

SCAR (Scientific Committee on Antarctic Research) (2012) *SCAR Antarctic Digital Database Version 6.0*. Scientific Committee on Antarctic Research, Cambridge. Digital media: http://www.add.scar.org

Shepherd A and 46 others (2012) A reconciled estimate of ice-sheet mass balance. *Science*, **338**(6111), 1183–1189 (doi: 10.1126/science.1228102)

Steinhage D, Nixdorf U, Meyer U and Miller H (1999) New maps of the ice thickness and subglacial topography in Dronning Maud Land, Antarctica, determined by means of airborne radio-echo sounding. *Ann. Glaciol.*, **29**, 267–272 (doi: 10.3189/172756499781821409)

Steinhage D, Nixdorf U, Meyer U and Miller H (2001) Subglacial topography and internal structure of central, western Dronning Maud Land, Antarctica, determined from airborne radio echo sounding. *J. Appl. Geophys.*, **47**(3–4), 183–189 (doi: 10.1016/S0926-9851(01)00063-5)

Van Autenboer T and Decleir H (1978) Glacier discharge in the Sør-Rondane, a contribution to the mass balance of Dronning Maud Land, Antarctica. *Z. Gletscherkd. Glazialgeol.*, **14**(1), 1–16

Van de Berg WJ, Van den Broeke MR, Reijmer CH and Van Mekjgaard E (2006) Reassessment of the Antarctic surface mass balance using calibrated output of a regional atmospheric climate model. *J. Geophys. Res.*, **111**(D11), D11104 (doi: 10.1029/2005JD006495)

Van Wessem JM and 13 others (2014) Improved representation of East Antarctic surface mass balance in a regional atmospheric climate model. *J. Glaciol.*, **60**(222), 761–770 (doi: 10.3189/2014JoG14J051)

Zwally HJ and Giovinetto MB (2011) Overview and assessment of Antarctic ice-sheet mass balance estimates: 1992–2009. *Surv. Geophys.*, **32**(4–5), 351–376 (doi: 10.1007/s10712-011-9123-5)